Microstructure and thermoelectric properties of Al-doped ZnO ceramic prepared by spark plasma sintering

Precious Manti Radingoana [a,d], Sophie Guillemet-Fritsch [a,*], Jacques Noudem [b], Peter Apata Olubambi [c], Geoffroy Chevallier [a], Claude Estournès [a]

[a] CIRIMAT, Université de Toulouse, CNRS, Université Toulouse, 3 - Paul Sabatier, 118 Route de Narbonne, 31062 Toulouse cedex 9, France
[b] Normandie Univ, Ensicaen, Unicaen, CNRS, CRISMAT, 14000 Caen, France
[c] University of Johannesburg, School of Mining, Metallurgy and Chemical Engineering, Johannesburg, South Africa
[d] Advanced Materials Manufacturing, Manufacturing Cluster, Council for Scientific and Industrial Research, P.O. Box 395, Pretoria 0001, South Africa

ARTICLE INFO

ZnO
Aluminum
Thermoelectric properties
Spark plasma sintering
Ceramics

ABSTRACT

The high thermal and low electrical conductivities of ZnO ceramics have hindered their thermoelectric applications. The doping of ZnO with group 3 elements can enhance the thermoelectric properties. In this work, Al (2 at%) doped ZnO powder was sintered using spark plasma sintering at varying parameters (such as temperature (550–700 °C), pressure (250–500 MPa) and the temperature of pressure application (Room Temperature (RT) and Holding Time (HT))). Maximum relative density of 98.9% was achieved at a temperature and pressure of 650 °C and 250 MPa, respectively. The Al-doped ZnO ceramics improved in electrical conductivity which caused a decrease in the Seebeck coefficient because of increased carrier concentration. The reduction in the grain size due to inhibiting growth effects of aluminum lead to a decrease in the thermal conductivity through phonon scattering at the grain boundaries. Hence, ZT of 0016 at 500 °C was obtained. This study indicated that Al-doped ZnO ceramics can be sintered at very low temperature of 650 °C. These conditions allow to retain the nanostructure, which is beneficial in improving the thermoelectric properties.

1. Introduction

Over the years, there has been a great progress in the thermoelectric performance of n-type ZnO based ceramics (such as Group 3 elements doping, polymer insertion, morphology modification etc....) [1–8]. We recently reported on the thermoelectric properties of pure zinc oxide (ZnO) [9]. According to the literature, doping ZnO with group 3 elements (such as aluminum (Al), gallium (Ga), indium (In)) can lead to enhanced electrical properties because dopants can modify the band gap of the oxide. Furthermore, their ionic radius are close to that of Zn (Al^{3+} 0.054 nm, In^{3+} 0.08 nm, Ga^{3+} 0.062 nm, Zn^{2+} 0.074 nm) [10,11]. Therefore, the ZnO structure will remain the same and the doping may generate free electrons in the conduction band.

Thus far, the highest ZT reported for doped ZnO ceramics is from dual doping of Al and Ga; ZT 0.45 @ 1000 K and ZT 0.65 @ 1247 K obtained using conventional sintering [12]. Al-doped ZnO ceramics were extensively investigated with ZTs of ~ 0.17–0.47 at 1000 K from ceramics prepared through hot press [12–15], microwave [16] and spark plasma sintering [17–22]. The substitution of Al on the zinc site of ZnO helps to improve thermoelectric properties through enhanced electrical conductivity and reduced thermal conductivity caused by nanostructuring. Aluminum is known to be a grain growth inhibitor [23,24].

However, these properties can be easily affected by the preparation methods of the doped powders. In most reported works, the authors have prepared them by solid state reactions of ZnO and Al_2O_3 raw powders which can cause inhomogeneity in the material [25]. The most reliable technique is the synthesis of the powders by wet chemical methods that lead to a homogenous mixture [26,27]. Nowadays, consolidation is being conducted using spark plasma sintering (SPS) technique; resulting in full densification which is attained in a short period which minimizes grain growth [28–30]. Smaller grains are effective for reducing thermal conductivity through phonon scattering [31,32] and increasing the Seebeck Coefficient [16,33]. So, bulk materials with smaller grains provide the most promising thermoelectric properties.

Recently, Cold Sintering Process (CSP) [34–37], Low temperature SPS/FAST [38,39] and Functional Graded Materials (FGM) [40,41] were

* Corresponding author.
E-mail address: sophie.guillemet@univ-tlse3.fr (S. Guillemet-Fritsch).

https://doi.org/10.1016/j.jeurceramsoc.2022.10.034

reported to control the grain size of bulk materials. In cold sintering process, small fraction of water and/or aqueous solution is added into powder to assist with densification of ceramics at very low temperatures of ~200 °C, as a result, the nanostructure of the material is maintained [37]. FGM improves the efficiency and temperature range of TE materials through continuous grain size gradient [40]. For instance, FGM Al-doped ZnO (0–5 wt% Al) layered ceramic prepared using SPS at 1000 °C. The simulated efficiency indicated that FGM has wider density range, and higher efficiency [41]. However, impurity phase, $ZnAl_2O_4$, was observed in the ceramic which has a huge impact on the resistivity. This result is in accordance with other work reported for Al-doped ZnO ceramics prepared by SPS, showing that the presence of spinel phase is problematic for resistivity value [17,19,20,22]. So, avoiding the spinel phase is desirable for higher electrical conductivity.

During SPS the thermal distribution is determined by the current density that has a great influence on the grain size, concentration of impurity phases (e.g $ZnAl_2O_4$) and dislocation defects [42–44]. For instance, sintering with high current density in Al-doped ZnO ceramics contributes to refined grain size and enhanced concentration of impurity phase, $ZnAl_2O_4$ [42]. Chen et al. [45] reported that sintering in low oxygen partial pressure leads to better substitution of Al ions into the ZnO lattice as compared to high oxygen partial pressure where it is transformed into spinel phase. Therefore, great attention needs to be taken when setting sintering conditions (such as temperature, current density, pressure, atmosphere etc.) to densify the Al-doped ZnO ceramics. Hence, a better understanding of the influence of SPS parameters on the microstructure and the thermoelectric properties of these ceramics is needed.

In this present work, ZnO was doped with 2 *mol%* Al. This choice was driven by the previously reported high ZT (0.3 – 0.45) at temperatures of about 1000 K for this composition, due to high electrical conductivity and reduced thermal conductivity [12,19,22]. The $Zn_{0.98}Al_{0.02}O$ powder was synthesized through co-precipitation followed by calcination. The sintering was performed using Spark plasma Sintering (SPS) at varying temperatures, pressures and point of pressure application to reach full densification and suitable microstructure. This discussion includes the description of the structure, the microstructure (relative density, grain size), and their influence on the thermoelectric properties of the Al-doped ZnO polycrystalline materials.

2. Materials and methodology

2.1. Synthesis of $Zn_{0.98}Al_{0.02}O$ powder

Al-doped ZnO powder was synthesized through the wet chemical method. Basically, the co-precipitation techniques followed by calcination, similarly to the procedures previously developed by Guy et al. [46,47]. Solutions of 4 M concentration of zinc nitrate hexahydrate and aluminum nitrate, and 0.2 M and 0.38 M ammonium oxalate monohydrate were prepared. Aluminum nitrate was added at an excess of 10% to ensure final aluminum concentration of 2 mol%. At ambient temperature, zinc nitrate hexahydrate/aluminum nitrate solution was mixed with 0.2 M ammonium oxalate monohydrate solution to initiate nucleation. At a subsequent time and constant stirring, 0.38 M ammonium oxalate monohydrate solution was added into the mixture to promote particle growth. The pH around 6.5–7 was adjusted using ammonia solution. The oxalate had the form of a white precipitate. After centrifugation, the product was dried at 80 °C during for 22 h, thereafter, calcined at 600 °C to form $Zn_{0.98}Al_{0.02}O$ powder.

2.2. Spark plasma sintering of the $Zn_{0.98}Al_{0.02}O$ powder

Al-doped ZnO powders were densified under air atmosphere with a Dr. Sinter 2080 unit (SPS Syntex Inc., Japan) available at the Plateforme Nationale de Frittage Flash (PNF2) located at the Université Toulouse 3 Paul Sabatier using tungsten carbide molds with 8 and 20 mm inner diameters. Prior to their filling with the powder, the molds were lined with 0.2 mm thick graphite foil (PERMAFOIL®Toyo Tanso). A pre-compaction step at 25 MPa for 1 min was systematically applied before the thermal cycle to ensure the same initial green state for all the samples. The influence of sintering temperature (550–700 °C), pressure (250–500 MPa) and point of applied pressure (room temperature (RT) or at the setpoint temperature (HT- Holding time) was investigated. The sintered ceramics were polished by silicon carbide discs (P320 and P600) to remove graphite foil for further characterizations.

2.3. Characterization techniques

2.3.1. Dense ceramics

The particle size and the morphology of the starting powders and the microstructure of the dense ceramics were investigated using Scanning Electron Microscopy (MEB JEOL JSM65 10LV and SEM-FEG (FEI HELIOS 600i). X-ray diffractometer (XRD Bruker D4) was used to analyse the phase structure. The surface area and particle size distribution were conducted using Brunauer–Emmett–Teller technique (BET) (Micromeritics desorb 2300 A) and the mastersizer (Mastersizer 2000 (CRISMAT) and Mastersizer 3000 (CIRIMAT)), respectively.

Electrical properties.

The electrical measurements were conducted at the Laboratoire de Cristallographie et Sciences des Matériaux (CRISMAT, UMR 6508 CNRS, CAEN France). Seebeck coefficient and resistivity of the dense ceramics were simultaneously measured using ZEM-3 (Ulvac-Riko) in argon atmosphere. The dense ceramics were cut into 9×3x3 mm bars and coated with gold to ensure electrical ohmic contact. Graphite foil was inserted on both sides of heaters to ensure a good electrical and thermal contact with the sample. The thermal conductivity was determined by measuring separately thermal diffusivity (α), ceramic density (d) and heat capacity (Cp) (Eq.01). The samples were cut into dimensions of 6×6x1 mm.

$$k \quad \alpha(T)\mathrm{Cp(T)d(T)} \tag{1}$$

The band gap was determined on ceramics of diameter 20 mm and thickness 0.5 mm, through the photovoltaic route using Bentham PVE 300 PV. The Hall Effect measurements were performed on 3 × 3 mm square samples using a commercial physical property measurement system (Model 7100 AC transport controller, Quantum Design).

3. Results and discussion

3.1. Spark plasma sintering of A l doped ZnO powder

The Al-doped ZnO powder ($Zn_{0.98}Al_{0.02}O$) was sintered by SPS in air at various parameters such as temperature, pressure and point of pressure application in order to get fully dense ceramics. Indeed, it has been previously shown that the use of WC tools allows to process oxide materials by SPS under air atmosphere and to overcome the problem of reduction due to the low oxygen partial pressure (neutral atmosphere, graphitic environment or dynamic vacuum) commonly encountered [48,49]. As a consequence, the annealing treatment, usually performed around 800 °C, is not necessary to re-oxidized the specimen which could induce grain growth. The summary of the ceramics characteristics for different sintering conditions are given in Table 1.

3.1.1. Sintering behavior of Al-doped ZnO ceramics

The shrinkage curves of the pure ZnO and the *2 at%* Al doped powders are given in Fig. 1. The shrinkage of both samples increased sharply till 550 °C. The sintering steps of *2 at%* Al-doped ZnO can be divided into three segments; the first stage is the rearrangement of the nanoparticles due to applied pressure. The displacement of *2 at%* was slow and reached only 0.7 mm as compared to 1.2 mm for *0 at%*, could be related to the aggregates present in the powder. The second stage is related to the progressive breaking of the remaining agglomerates and/

Table 1
Summary of pure and Al-doped ZnO ceramics characteristics for varied SPS parameters (*Note: RT-Room Temperature, HT- Holding time Temperature*).

Ref.	Temperature	Initial Pressure	Final Pressure	Point of Pressure application	Atmosphere	Relative density	Grain size
	°C	MPa	MPa	°C		%	μm
ZnO							
1	600	25	250	RT	Air	99.3 ± 0.1	2.4 ± 0.6
2	700	25	250	RT	Air	100	5 ± 2
$Zn_{0.98}Al_{0.02}O$							
3	RT	250	250	RT	Air	57 ± 0.2	–
4	550	250	250	RT	Air	79.9 ± 0.5	–
5	600	250	250	RT	Air	84.9 ± 0.2	–
6	650	250	250	RT	Air	98.9 ± 0.1	0.46 ± 0.01
7	700	25	250	RT	Air	98.1 ± 0.1	0.76 ± 0.26
8	600	25	250	HT	Air	84.3 ± 0.2	–
9	650	25	250	HT	Air	98.6 ± 0.1	0.26 ± 0.01
10	600	100	500	HT	Air	98.5 ± 0.1	–
[$Zn_{0.98}Al_{0.02}O$] Bibliography							
Ma et al. [54]	900	50	50	–	Vacuum	99.9	–
Nam et al. [19]	900	50	50	–	Vacuum	94	0.2
Han et al. [18]	950	50	50	–	Vacuum	90	–

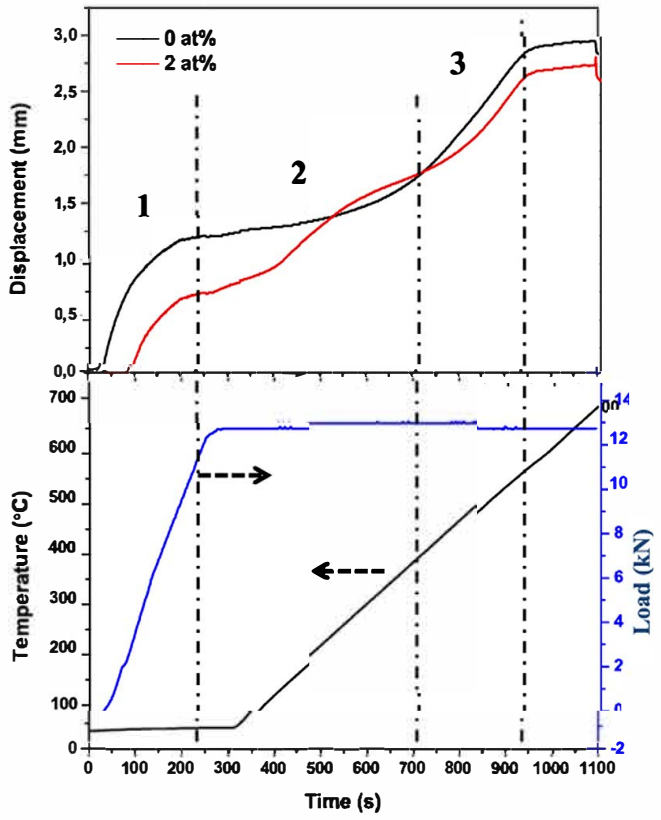

Fig. 1. Sintering behavior of pure ZnO and Al-doped ZnO using spark plasma sintering.

or to the neck formations between the particles due to localized heating caused by spark discharge [26,28,50,51]. The third stage is related to extend of the neck's formation between the particles and to the densification step with progressive pore elimination. After 550 °C, the slight increase in displacement of both samples could be due to final densification with elimination of the residual pores [52]. The total displacement between these samples differed by 0.5 mm. This difference can be related to the influences of grain size on the sintering behavior of the ceramics. The higher density of grain boundaries in the doped sample compared with the pure ZnO could have enhanced the diffusion rate [53], as visible in zone 2 where the kinetics are higher. As a result, the optimal sintering temperature decreased. The reduction in the sintering temperature has been reported on the sintering of nanoparticles materials such as ZnO [28,38,39]. Reduced temperature implies less grain growth and more grains boundaries, which will be beneficial for improving thermoelectric properties. The relative densities of the ceramics are given in Table 1 for the different sintering temperatures (from 550 °C to 700 °C).

3.1.2. *Effect of sintering temperatures*

The influence of the sintering temperature (550–700 °C) on the structure, the microstructure, and the density of Al-doped ZnO ceramics was studied. Relative density versus temperature given in Fig. 2 showed an increase in the relative density with an increment in the temperature. Maximum relative density of 98.9% was achieved at 650 °C, with initial relative green density of 57% at room temperature. Beyond 650 °C a decrease in the relative density was observed which could be due to the presence of pores and/or decrease in the ceramic density related to the physical properties such as the density of the individual materials [54,55]. The XRD patterns of the Al doped ZnO ceramics are given in Fig. 3. For instance, at 700 °C the concentration of secondary phases increases. This phase has a lower density as compared to that of ZnO. The sum of the total density of the ceramic will drop. Ma et al. [54] reported higher densification rate (i.e. 99.9%) but such level was obtained after sintering in reduced atmosphere for higher sintering temperature (i.e. 900 °C) than the range explored in the present study. Nam et al. [19] and Han et al. [18] reported lower relative densities of 94% and 90% at temperatures of 900 °C and 950 °C, respectively, after sintering in vacuum.

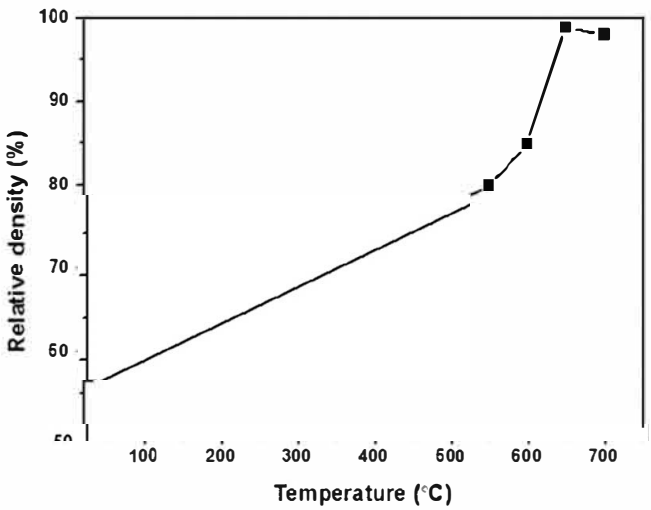

Fig. 2. Relative density versus temperature of Al-doped ZnO ceramics.

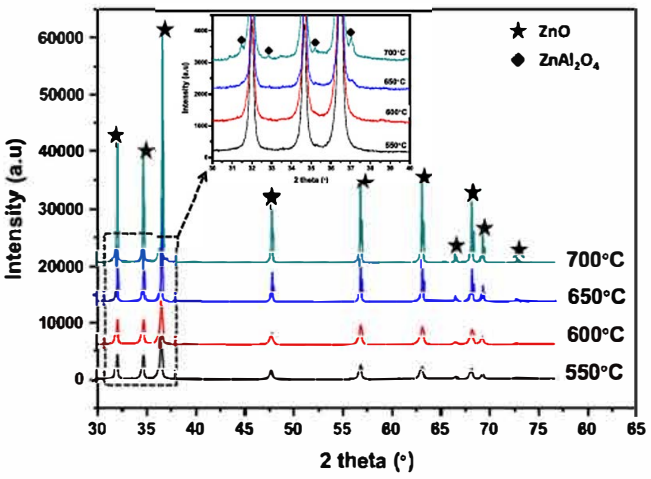

Fig. 3. XRD patterns of Al-doped ZnO ceramics at varying temperature.

Other reports mentioned relative densities of 99% at temperatures between 800 and 1200 °C and only 65–93%, for lower sintering temperature, 700–900 °C for Al-doped ZnO ceramics [17,56]. In the present study we want to point out that a high relative density of 98.9% was obtained at a temperature of only 650 °C and high pressure of 250 MPa. The achievement of such high relative density at low temperature could be due to the combination of high reactivity of the powders (i.e. small grain size), better rearrangement of the grains, and higher pressure applied.

The analysis of the XRD patterns of most of the Al-doped ZnO ceramics (Fig. 3) showed that the main phase corresponds to the ZnO hexagonal Wurzite structure. It was observed that as the sintering temperature increases the XRD peaks of the ceramics are sharpened which is related to the increase in the grain size. The zoomed inserted image indicated the presence of spinel phase ($ZnAl_2O_4$) with very small peaks at 37°, 35°, 32.5° and 31.5°. This indicates that during the sintering at low temperatures, in air, there is efficient incorporation of Al ions in ZnO lattice. At high temperature demixion occurs that leads to the formation of the spinel phase. According to Ellingham's phase diagram [58], low partial pressure of oxygen promotes further substitution of Al into the ZnO structure. Whereas, at high oxygen partial pressure, excess Al reacts with ZnO to form $ZnAl_2O_4$. Our data are in line with reported work of Chen *et al.* [42], on the microstructure difference between conventional and SPS of Al-doped ZnO ceramics sintered at 1200 °C in air and 1000 °C in vacuum. It was found that the samples exposed to air had high concentration of spinel phase compared to those in vacuum due to the differences in oxygen partial pressure and rapid dissolution of Al ions into ZnO lattice caused by the high DC current applied in SPS process. Similarly, higher concentration of spinel phase was observed in air than in nitrogen atmosphere prepared using conventional route at 1400 °C for Al-doped ZnO ceramic[57]. Nunes and Bradt [58] reported on conventionally sintered $ZnO/Bi_2O_3/Al_2O_3$ ceramics and determined an activation energy of 400 kJ/mol for ZnO grain growth. So, the transport of the $ZnAl_2O_4$ spinel particles is most probably controlled by the diffusion of O^{2-} ions in the $ZnAl_2O_4$ spinel structure.

The secondary phase present in higher quantity at higher temperature contributes to the decrease of the total relative density of the samples sintered at 700 °C, since the density of $ZnAl_2O_4$ phase (i.e. 4.61 g/cm^3) is lower than the one of ZnO (i.e. 5.61 g/cm^3).

The SEM micrograph of *0 at%* and 2 at% Al doped ZnO ceramics sintered at 700 °C are given in Fig. 4. A significant decrease in the grain size is observed in the doped ZnO with 2 at% Al (i.e. 0.76 μm, Fig. 4c) compared to pure ZnO (i.e. 5.8 μm, Fig. 4(a). This could be due to the grain growth inhibiting effects of aluminum as discussed in previous sections. Further studies were done to understand the influence of sintering temperature on the microstructure of 2 at% Al doped ZnO. It was observed that sintering at 550 °C and 600 °C did not change the grain size of the ceramics. However, at a temperature of 650 °C and 700 °C the grain size increased from initial grain size of 75–457 nm and 760 nm, respectively, (see Fig. 4 ((c) and (d)). EDX analysis (Fig. 4b) on the sample sintered at 700 °C indicated that the light phase is Al rich and the dark phase is Zn rich. Therefore, the light phase observed by SEM is the

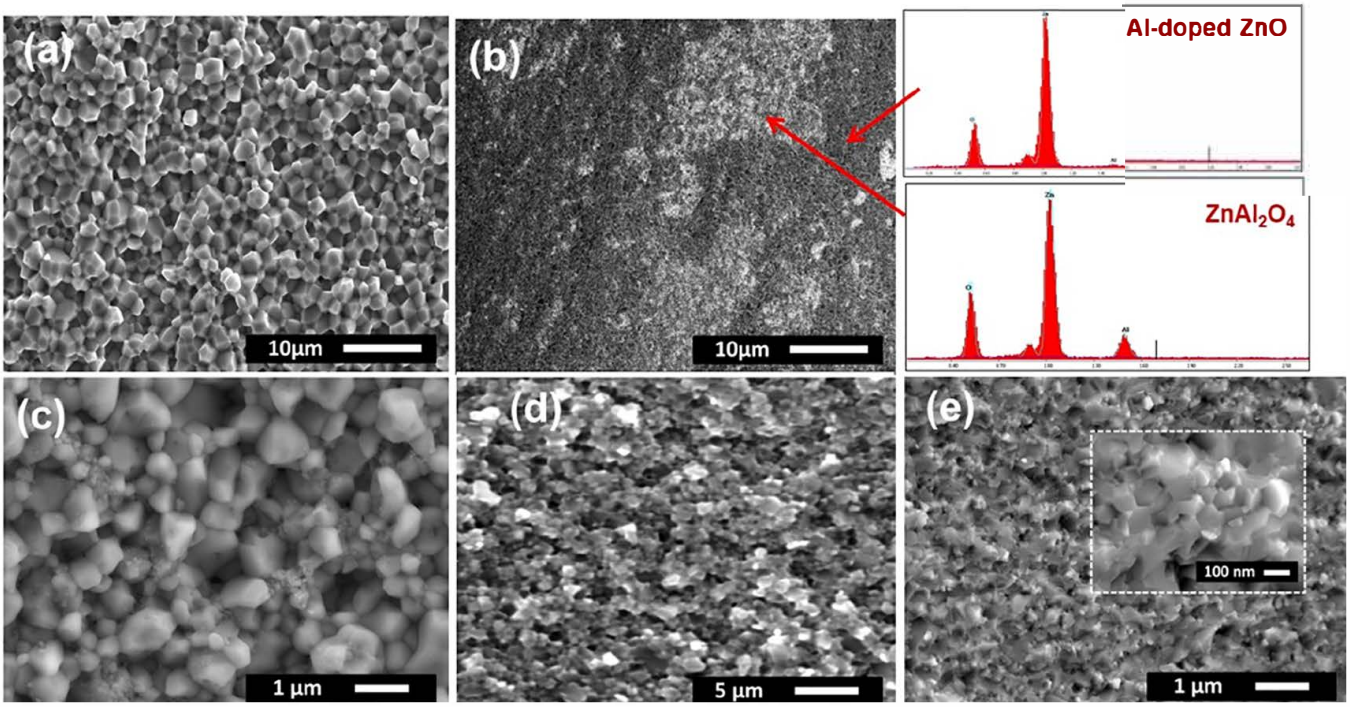

Fig. 4. SEM micrographs of 0 at% and 2 at% Al ZnO ceramic sintered at 700 °C and 650 °C (a) Pure ZnO (700-RT), (b) Al-ZnO with EDX analysis (700-RT) (c) Al-ZnO with grain structure (700-RT), (d) Al-ZnO (650-RT) and (e) Al-ZnO with zoomed part (650-HT).

spinel phase $ZnAl_2O_4$ as confirmed by XRD analysis. This result is in agreement with the work of Jood et al. [16]. The authors noticed that the spinel phase is homogeneously distributed across the sample. The presence of the spinel phase influences the electrical properties such as resistivity and carrier mobility. Some reports indicated that it could lead to a decrease of the thermal conductivity while on the other hand it could be a hindrance in improving the electrical conductivity due to electron scattering [13,16–19,25]. EDX analysis of the sample sintered at 650 °C did not indicate any secondary phases which may be attributed to the low concentration of $ZnAl_2O_4$. Further studies were conducted to reduce the concentration of secondary phase in the ceramics while keeping high densification.

3.1.3. *Reduction of the amount of spinel phase in Al-doped ZnO ceramics*

In the previous section, it was indicated that sintering at temperature above 650 °C with a pressure of 250 MPa applied at room temperature causes the formation of the secondary phases that can be a hindrance in improving thermoelectric properties. One way to avoid the presence of spinel phase in the sintered ceramics is to decrease the setpoint temperature below 650 °C while conserving the objective to obtain dense specimen. To do so two strategies have been followed: the first one is to apply the high pressure at the holding point/temperature (HT) and the second one is to double the pressure. At first the influence of the changes in sintering conditions on the densification was determined. For a set point temperature of 600 °C, the relative densities of the samples reached only 84% even though a pressure of 250 MPa is applied at room temperature and at the dwell (HT), see Table 1. An increase in the relative density from 84% to 98.5% was observed when the sintering pressure was increased to 500 MPa during heating stage at a temperature of 600 °C. However, the sintered ceramic cracked at this pressure due to distribution of residual stresses during cooling of sintered ceramic [59]. So, an optimal densification of 98.6% was achieved at 650 °C and 250 MPa without cracks. This high densification will be beneficial in improving the electrical conductivity and better thermoelectric properties.

The XRD patterns of the ceramics sintered at different temperatures and point of applied pressure are reported in Fig. 5. For all the samples, the major phase present is hexagonal ZnO, the same structure as the powder. The secondary $ZnAl_2O_4$ phase is noticed for the sample sintered at 650 °C when the pressure is applied at room temperature (RT). Applying the pressure during the dwell time (HT) allows to avoid the formation of the spinel phase at 650 °C. In this case, we suppose that the application of pressure at HT is an additional parameter that promotes the diffusion of Al atoms in the ZnO structure [42].

SEM-FEG micrograph of the sample sintered at 650 °C using HT mode (Fig. 4(e)) revealed a decrease in the grain size from 457 nm to 260 nm as compared to the sample sintered using RT mode. The differences in heat transfer between the grains could have caused the grain size difference; RT mode had better contact as compared to HT mode [51]. This polycrystalline sample was further annealed in air at 600 °C for 24 h (not shown) to obtain fully oxidized ceramic and ensure stable measurement and reproducibility of electrical properties. XRD and SEM analysis of the annealed sample did not show any significant changes in the phase structure and the grain size.

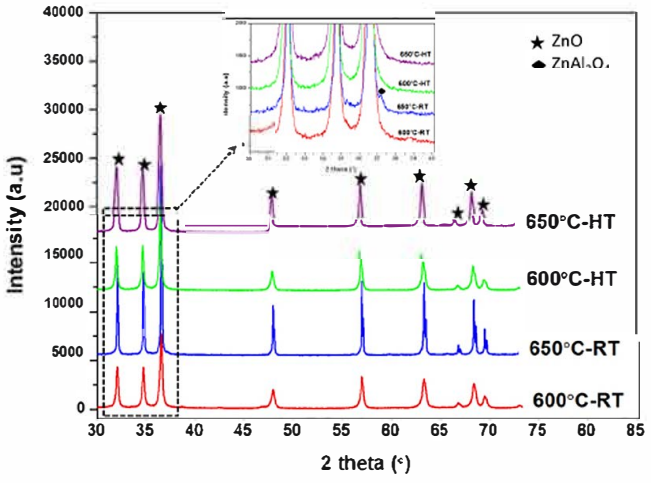

Fig. 5. XRD patterns of Al-doped ZnO ceramics sintered at 600 °C and 650 °C with a pressure of 250 MPa using RT and HT mode.

3.2. *Thermoelectric properties*

The thermoelectric properties were determined for the annealed ceramic sintered at 650 °C (HT) as it contains minimal/no secondary phase and exhibit a relative density of 98.6%. see Fig. 6. The resistivity as a function of temperature is given in Fig. 6(a); for the samples *0 at%* and *2 at%*. It is shown that addition of Al in ZnO reduces the resistivity especially at low temperature (< 200 °C). At 50 °C the resistivity reduced from ~197 Ω.cm to ~0.46 Ω.cm for *0 Al at%* and 2 Al *at%*, respectively. This difference is attributed to the substitution of Al^{3+} ions on the Zn^{2+} site creating extra free electrons [17–22]. It is observed that the resistivity of both samples decreases with an increase in temperature, which is significant of a semiconducting behavior. At high temperature the valence electrons gain enough energy to reach the conduction band, hence, the lowest resistivity of about 0.03 Ω.cm at 500 °C [60]. Søndergaard et al. [61] reported a lower resistivity compared to our samples for the same Al content, i.e. resistivity values of 0.005 and 0.0015 Ω.cm at room temperature were obtained for samples sintered at 850 °C and 900 °C, respectively, using spark plasma sintering in vacuum. This difference is probably due to high carrier concentration caused by differences in preparation methods and particularly the annealing treatment after sintering. Søndergaard et al. [61] performed an annealing treatment in air for a week at 800 °C while in our case, the treatment was chosen at much lower temperature, to avoid the grain growth, i.e. 600 °C (because of lower sintering temperature) for 24 h in air also. Obviously, the annealing at 800 °C for such a long time leads to the creation of more oxygen vacancies that significantly reduce the resistivity.

The Seebeck Coefficient as a function of temperature is given in Fig. 6 (b). The negative sign indicates and confirms the *n-type* conductivity. Adding 2 *at%* Al reduced the Seebeck coefficient value from 800 to 175 μV/K at 50 °C. This decrease could be caused by the increase in the carrier concentration. The broadband Eq. (1) indicates inverse relationship between Seebeck coefficient and carrier concentration [62].

$$S_{bulk} \quad \frac{8m^*\pi^2k_b^2}{3eh^2}T\left(\frac{\pi}{3n}\right)^{\frac{2}{3}} \tag{2}$$

The absolute Seebeck Coefficient, |S|, for the *2 Al at%* sample increases with an increase in temperature from 50 °C to 500 °C; which is related to the scattering of the electrons at high temperature. The behaviour is different from pure ZnO which showed a decrease in the |S| with temperature increment. Søndergaard et al.[61] reported similar behaviour to that of 2 at% Al-doped ZnO with |S| of about 125 μV/K at 50 °C for sintering at 850 °C and 900 °C.

The temperature dependence of the thermal conductivity of the polycrystalline ceramic presented in Fig. 6(c) revealed that doping with Al into ZnO ceramic reduces the thermal conductivity from 47 W/m.K (0 at%) to 27 W/m.K (2 at%) at 50 °C. This was caused by phonon scattering at the grain boundaries because of reduced grain size [17–22]. It is clearly shown that the thermal conductivity determined in this present work is almost similar to that reported by Søndergaard et al.[61] probably because of similar grain size.

The performance of the ceramics was determined using figure of merit, ZT, given in Fig. 6(d). An increase in ZT was observed with temperature increment for all samples. It was observed that *0 at%* performs better than the *2 at%* ceramic by a ZT value of 0029 at a

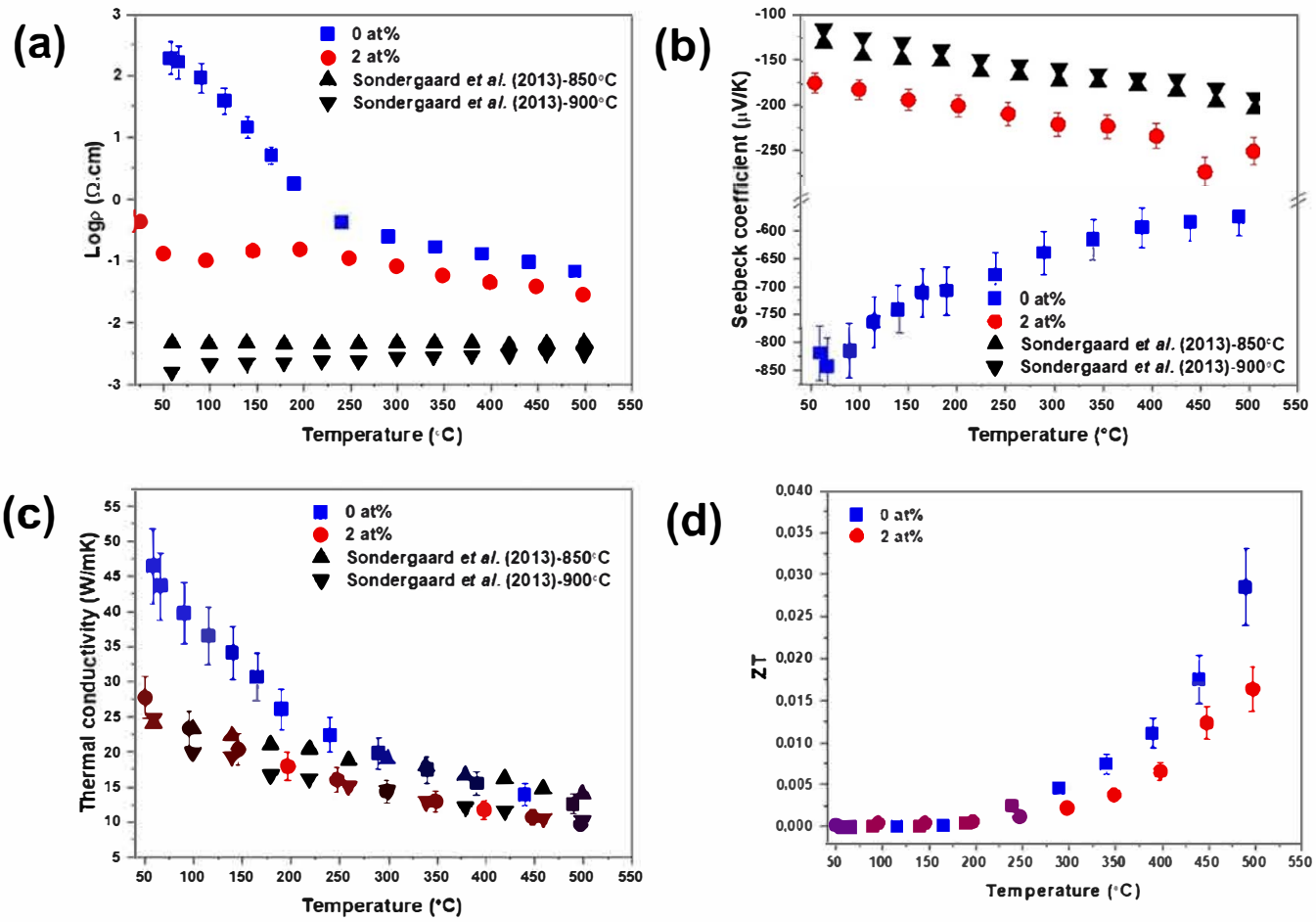

Fig. 6. Thermoelectric properties of annealed pure and Al-doped ZnO ceramic sintered at 650 °C (HT): (a) Resistivity (b) Seebeck Coefficient (c) Thermal conductivity (d) Figure of merit (ZT).

temperature of 500 °C. The improved performance is because of high Seebeck Coefficient shown by *0 at%* ceramics. The performance of the *2 at%* can be enhanced by improving the solubility of Al in ZnO through process manipulations such as sintering temperature increment and operating in vacuum to increase the electrical conductivity. Also, new materials could be incorporated with the Al-doped ZnO ceramic to enhance the electrical conductivity and seebeck coefficient while maintaining the nanostructure of ceramic.

4. Conclusions

The synthesis and spark plasma sintering of Al-doped ZnO powder was described. The addition of 2 at% Al in ZnO powder reduces the grain size from 177 to 75 nm. The relative density of Al-doped ZnO sintered at a temperature of 650 °C reaches high relative density of 98.9%. Sintering above 650 °C causes an increase in the grain size which consequently decreases the relative density due to the presence of pores. The addition of Al into the ZnO ceramics caused a decrease in the grain size from 5.4 μm (without Al) to < 470 nm (with 2 at% Al). Sintering above 650 °C and applying the axial pressure during room temperature leads to the formation of the spinel phase, $ZnAl_2O_4$, which is unwanted for thermoelectric properties. Applying the pressure during holding time prevents the formation of spinel phase. The concentration of spinel phase is influenced by the oxygen partial pressure. The resistivity of the Al-doped ZnO ceramics slightly reduces, which causes a decrease in the absolute Seebeck Coefficient as a result of increased carrier concentration. The reduction in the grain size leads to a decrease in the thermal conductivity due to phonon scattering at the grain boundaries. As a result, ZT value of 0016 at 500 °C, smaller than the one of pure ZnO ceramics was obtained. The low Seebeck Coefficient and electrical conductivity value of Al-doped ZnO ceramic caused the decrease in the performance. Even so, these results revealed the importance of reduced thermal conductivity and low resistivity to improve the thermoelectric properties of Al-doped ZnO ceramics. It is advised to do further experiments to optimize the amount of Al dopants in ZnO ceramics and maybe consider incorporation of new materials to develop new composites and/or play with oxygen stoichiometry by optimizing sintering and annealing parameters especially the operating atmosphere to improve thermoelectric properties.

Declaration of Competing Interest

The authors declare that they have no known competing financial interests or personal relationships that could have appeared to influence the work reported in this paper.

Acknowledgements

This project was funded by A European and South African Partnership on Heritage and Past+ (AESOP+, Europe) (551128-EM-1–2014-1-FR-ERA MUNDUS-EMA21) and National Research Fund (NRF, South Africa) (102699). The authors would like to thank Y. Borjon-Piron (CIRIMAT) for SEM observations, and J. Lecourt, F. Veillon and C. Bilot from CRISMAT laboratory for their technical assistance.

[1] J.W. Fergus, Oxide materials for high temperature thermoelectric energy conversion, J. Eur. Ceram. Soc. 32 (3) (2012) 525–540, https://doi.org/10.1016/j.jeurceramsoc.2011.10.007.

[2] Y. Feng, X. Jiang, E. Ghafari, B. Kucukgok, C. Zhang, I. Ferguson, N. Lu, Metal oxides for thermoelectric power generation and beyond, Adv. Compos. Hybrid. Mater. (2017) 1–13, https://doi.org/10.1007/s42114-017-0011-4.

[3] B. Zhu, C. Chen, Z. Yao, J. Chen, C. Jia, Z. Wang, R. Tian, L. Tao, F. Xue, H. Hng, Multiple doped ZnO with enhanced thermoelectric properties, J. Eur. Ceram. Soc. 41 (7) (2021) 4182–4188, https://doi.org/10.1016/j.jeurceramsoc.2021.01.054.

[4] M. Mitra, K. Kargupta, S. Ganguly, S. Goswami, D. Banerjee, Facile synthesis and thermoelectric properties of aluminum doped zinc oxide/polyaniline (AZO/PANI) hybrid, Synth. Met. 228 (2017) 25–31, https://doi.org/10.1016/j.synthmet.2017.03.017.

[5] Z.-H. Wu, H.-Q. Xie, Y.-B. Zhai, Enhanced thermoelectric figure of merit in nanostructured ZnO by nanojunction effect, Appl. Phys. Lett. 103 (24) (2013), 243901, https://doi.org/10.1063/1.4842035.

[6] Y. Wu, D.-B. Zhang, Z. Zhao, J. Pei, B.-P. Zhang, Enhanced thermoelectric properties of ZnO: C doping and band gap tuning, J. Eur. Ceram. Soc. 41 (2) (2021) 1324–1331, https://doi.org/10.1016/j.jeurceramsoc.2020.09.042.

[7] A. Fedotov, A. Pashkevich, J. Fedotova, A. Fedotov, T. Kołtunowicz, P. Zukowski, A.A. Ronassi, V. Fedotova, I. Svito, M. Budzyński, Electron transport and thermoelectric properties of ZnO ceramics doped with Fe, J. Alloy. Compd. 854 (2021), 156169, https://doi.org/10.1016/j.jallcom.2020.156169.

[8] N. Baghdadi, N. Salah, A. Alshahrie, A. Ansari, K. Koumoto, The effect of morphological modification on the thermoelectric properties of ZnO nanomaterials, Ceram. Int. 47 (5) (2021) 6169–6178, https://doi.org/10.1016/j.ceramint.2020.10.195.

[9] P.M. Radingoana, S. Guillemet-Fritsch, J. Noudem, P.A. Olubambi, G. Chevallier, C. Estournès, Thermoelectric properties of ZnO ceramics densified through spark plasma sintering, Ceram. Int. 46 (4) (2020) 5229–5238, https://doi.org/10.1016/j.ceramint.2019.10.271.

[10] V.K. Jayaraman, A.M. Álvarez, Y.M. Kuwabara, Y. Koudriavstev, Effect of co-doping concentration on structural, morphological, optical and electrical properties of aluminium and indium co-doped ZnO thin films deposited by ultrasonic spray pyrolysis, Mater. Sci. Semicond. Process. 47 (2016) 32–36, https://doi.org/10.1016/j.mssp.2016.02.011.

[11] D.C. Look, Progress in ZnO materials and devices, J. Electron. Mater. 35 (6) (2006) 1299–1305, https://doi.org/10.1007/s11664-006-0258-y.

[12] M. Ohtaki, K. Araki, K. Yamamoto, High thermoelectric performance of dually doped ZnO ceramics, J. Electron. Mater. 38 (7) (2009) 1234–1238, https://doi.org/10.1007/s11664-009-0816-1.

[13] T. Tsubota, M. Ohtaki, K. Eguchi, H. Arai, Thermoelectric properties of Al-doped ZnO as a promising oxide material for high-temperature thermoelectric conversion, J. Mater. Chem. 7 (1) (1997) 85–90, https://doi.org/10.1039/a602506d.

[14] M. Ohtaki, T. Tsubota, K. Eguchi, H. Arai, High-temperature thermoelectric properties of (Zn1− x Al x) O, J. Appl. Phys. 79 (3) (1996) 1816–1818, https://doi.org/10.1063/1.360976.

[15] Y. Fujishiro, M. Miyata, M. Awano, K. Maeda, Effect of microstructural control on thermoelectric properties of hot-pressed aluminum-doped zinc oxide, J. Am. Ceram. Soc. 86 (12) (2003) 2063–2066, https://doi.org/10.1111/j.1151-2916.2003.tb03610.x.

[16] P. Jood, R.J. Mehta, Y. Zhang, G. Peleckis, X. Wang, R.W. Siegel, T. Borca-Tasciuc, S.X. Dou, G. Ramanath, Al-doped zinc oxide nanocomposites with enhanced thermoelectric properties, Nano Lett. 11 (10) (2011) 4337–4342, https://doi.org/10.1021/nl202439h.

[17] D. Gautam, M. Engenhorst, C. Schilling, G. Schierning, R. Schmechel, M. Winterer, Thermoelectric properties of pulsed current sintered nanocrystalline Al-doped ZnO by chemical vapour synthesis, J. Mater. Chem. A 3 (1) (2015) 189–197, https://doi.org/10.1039/c4ta04355c.

[18] L. Han, N. Van Nong, W. Zhang, L.T. Hung, T. Holgate, K. Tashiro, M. Ohtaki, N. Pryds, S. Linderoth, Effects of morphology on the thermoelectric properties of Al-doped ZnO, RSC Adv. 4 (24) (2014) 12353–12361, https://doi.org/10.1039/c3ra47617k.

[19] W.H. Nam, Y.S. Lim, S.-M. Choi, W.-S. Seo, J.Y. Lee, High-temperature charge transport and thermoelectric properties of a degenerately Al-doped ZnO nanocomposite, J. Mater. Chem. 22 (29) (2012) 14633–14638, https://doi.org/10.1039/c2jm31763j.

[20] L. Han, High Temperature Thermoelectric Properties of ZnO Based Materials, Department of Energy Conversion and Storage, Technical University of Denmark, 2014.

[21] L. Han, N. Van Nong, L.T. Hung, T. Holgate, N. Pryds, M. Ohtaki, S. Linderoth, The influence of α-and γ-Al2O3 phases on the thermoelectric properties of Al-doped ZnO, J. Alloy. Compd. 555 (2013) 291–296, https://doi.org/10.1016/j.jallcom.2012.12.091.

[22] D.-B. Zhang, H.-Z. Li, B.-P. Zhang, M.Xia D.-d. Liang, Hybrid-structured ZnO thermoelectric materials with high carrier mobility and reduced thermal conductivity, RSC Adv. 7 (18) (2017) 10855–10864, https://doi.org/10.1039/c6ra28854e.

[23] Y. Zhang, W. Wang, R. Tan, Y. Yang, X. Zhang, P. Cui, W. Song, The solubility and temperature dependence of resistivity for aluminum-doped zinc oxide ceramic, Int. J. Appl. Ceram. Technol. 9 (2) (2012) 374–381, https://doi.org/10.1111/j.1744-7402.2011.02666.x.

[24] T. Teranishi, Y. Mori, H. Hayashi, A. Kishimoto, Thermoelectric property of polycrystalline aluminum-doped zinc oxide enhanced by micropore foaming, J. Am. Ceram. Soc. 95 (2) (2012) 690–695, https://doi.org/10.1111/j.1551-2916.2011.04837.x.

[25] K. Cai, E. Müller, C. Drašar, A. Mrotzek, Preparation and thermoelectric properties of Al-doped ZnO ceramics, Mater. Sci. Eng.: B 104(1-2) ((2003) 45-48, https://doi.org/10.1016/S0921-5107(03)00280-0.

[26] Y. Beynet, A. Izoulet, S. Guillemet-Fritsch, G. Chevallier, V. Bley, T. Pérel, F. Malpiece, J. Morel, C. Estournès, ZnO-based varistors prepared by spark plasma sintering, J. Eur. Ceram. Soc. 35 (4) (2015) 1199–1208, https://doi.org/10.1016/j.jeurceramsoc.2014.10.007.

[27] I. Guy, Elaboration and characterization of powders and varistors based on zinc oxide dope, Univ. Paul. Sabatier (1995) 201.

[28] R. Chaim, M. Levin, A. Shlayer, C. Estournès, Sintering and densification of nanocrystalline ceramic oxide powders: a review, Adv. Appl. Ceram. 107 (3) (2008) 159–169, https://doi.org/10.1179/174367508×297812.

[29] O. Guillon, J. Gonzalez-Julian, B. Dargatz, T. Kessel, G. Schierning, J. Rathel, M. Herrmann, Field-assisted sintering technology/spark plasma sintering: mechanisms, materials, and technology developments, Adv. Eng. Mater. 16 (7) (2014) 830–849, https://doi.org/10.1002/adem.201300409.

[30] R. Chaim, M. Levin, A. Shlayer, C. Estournès, Sintering and densification of nanocrystalline ceramic oxide powders: a review, Adv. Appl. Ceram. 107 (3) (2008) 159–169, https://doi.org/10.1179/174367508×297812.

[31] M. Holland, Phonon scattering in semiconductors from thermal conductivity studies, Phys. Rev. 134 (2A) (1964) A471, https://doi.org/10.1103/PhysRev.134.A471.

[32] F. Giovannelli, C. Chen, P. Díaz-Chao, E. Guilmeau, F. Delorme, Thermal conductivity and stability of Al-doped ZnO nanostructured ceramics, J. Eur. Ceram. Soc. 38 (15) (2018) 5015–5020, https://doi.org/10.1016/j.jeurceramsoc.2018.07.032.

[33] J.-F. Li, W.-S. Liu, L.-D. Zhao, M. Zhou, High-performance nanostructured thermoelectric materials, NPG Asia Mater. 2 (4) (2010) 152, https://doi.org/10.1038/asiamat.2010.138.

[34] S. Funahashi, J. Guo, H. Guo, K. Wang, A.L. Baker, K. Shiratsuyu, C.A. Randall, Demonstration of the cold sintering process study for the densification and grain growth of ZnO ceramics, J. Am. Ceram. Soc. 100 (2) (2017) 546–553, https://doi.org/10.1111/jace.14617.

[35] J. Gonzalez-Julian, K. Neuhaus, M. Bernemann, J.P. da Silva, A. Laptev, M. Bram, O. Guillon, Unveiling the mechanisms of cold sintering of ZnO at 250° C by varying applied stress and characterizing grain boundaries by Kelvin Probe Force Microscopy, Acta Mater. 144 (2018) 116–128, https://doi.org/10.1016/j.actamat.2017.10.055.

[36] H. Guo, A. Baker, J. Guo, C.A. Randall, Cold sintering process: a novel technique for low-temperature ceramic processing of ferroelectrics, J. Am. Ceram. Soc. 99 (11) (2016) 3489–3507, https://doi.org/10.1111/jace.14554.

[37] X. Jiang, G. Zhu, H. Xu, L. Dong, J. Song, X. Zhang, Y. Zhao, D. Yan, A. Yu, Preparation of high density ZnO ceramics by the Cold Sintering Process, Ceram. Int. 45 (14) (2019) 17382–17386, https://doi.org/10.1016/j.ceramint.2019.05.298.

[38] B. Dargatz, J. Gonzalez-Julian, M. Bram, P. Jakes, A. Besmehn, L. Schade, R. Roder, C. Ronning, O. Guillon, FAST/SPS sintering of nanocrystalline zinc oxide—Part I: Enhanced densification and formation of hydrogen-related defects in presence of adsorbed water, J. Eur. Ceram. Soc. 36 (5) (2016) 1207–1220, https://doi.org/10.1016/j.jeurceramsoc.2015.12.009.

[39] B. Dargatz, J. Gonzalez-Julian, M. Bram, Y. Shinoda, F. Wakai, O. Guillon, FAST/SPS sintering of nanocrystalline zinc oxide—Part II: Abnormal grain growth, texture and grain anisotropy, J. Eur. Ceram. Soc. 36 (5) (2016) 1221–1232, https://doi.org/10.1016/j.jeurceramsoc.2015.12.008.

[40] C.L. Cramer, J. Gonzalez-Julian, P.S. Colasuonno, T.B. Holland, Continuous functionally graded material to improve the thermoelectric properties of ZnO, J. Eur. Ceram. Soc. 37 (15) (2017) 4693–4700, https://doi.org/10.1016/j.jeurceramsoc.2017.07.019.

[41] C.L. Cramer, H. Wang, M.J. Lance, A.A. Trofimov, E. Cakmak, Z.-H. Jin, Testing and modeling of functionally graded aluminum-doped zinc oxide using spark plasma sintering and discrete powder layers of varying composition, Phys. Status Solidi (a) 219 (1) (2022), 2100483, https://doi.org/10.1002/pssa.202100483.

[42] S. Yang, F. Chen, Q. Shen, L. Zhang, A. Huang, H. Gu, Influence of electric current on microstructure and electrical property of Al-doped ZnO ceramic consolidated by spark plasma sintering, Ceram. Int. 46 (17) (2020) 26539–26547, https://doi.org/10.1016/j.ceramint.2020.07.120.

[43] S.M. Bagheri, M. Vajdi, F.S. Moghanlou, M. Sakkaki, M. Mohammadi, M. Shokouhimehr, M.S. Asl, Numerical modeling of heat transfer during spark plasma sintering of titanium carbide, Ceram. Int. 46 (6) (2020) 7615–7624, https://doi.org/10.1016/j.ceramint.2019.11.262.

[44] S. Yang, F. Chen, Q. Shen, L. Zhang, Microstructure and electrical property of aluminum doped zinc oxide ceramics by isolating current under spark plasma sintering, J. Eur. Ceram. Soc. 36 (8) (2016) 1953–1959, https://doi.org/10.1016/j.jeurceramsoc.2016.02.027.

[45] H. Chen, Q. Sun, T. Tian, L. Zheng, M. Barré, I. Monot-Laffez, M. Makowska-Janusik, G. Li, A.H. Kassiba, Defects and microstructure of highly conducting Al doped ZnO ceramics obtained via spark plasma sintering, J. Eur. Ceram. Soc. 40 (15) (2020) 5529–5534, https://doi.org/10.1016/j.jeurceramsoc.2020.06.030.

[46] I. Guy, Elaboration et caractérisation de poudres et de varistances à base d'oxyde de zinc dopé, Toulouse 3 (1995).

[47] J.-E. Mory, I. Guy, D. Schneider, A. Rousset, R. Legros, A. Peigney, Poudre d'oxyde de zinc dope, procede de fabrication et ceramique obtenue a partir de ladite poudre, in: P.C.D. FRANCE (Ed.) IFI CLAIMS PATENT SERVICES, Jean-Eudes

MoryIsabelle GuyDidier SchneiderAbel RoussetRenee LegrosAlain PeigneyPharmacie Centrale De France France, 1993.
[48] J.G. Noudem, S. Quetel-Weben, R. Retoux, G. Chevallier, C. Estournès, Thermoelectric properties of Ca0. 9Yb0. 1MnO3− x prepared by spark plasma sintering in air atmosphere, Scr. Mater. 68 (12) (2013) 949–952, https://doi.org/10.1016/j.scriptamat.2013.02.059.
[49] G. Philippot, M. Albino, R. Epherre, G. Chevallier, Y. Beynet, C. Manière, A. Weibel, A. Peigney, M. Deluca, C. Elissalde, Local distortions in nanostructured ferroelectric ceramics through strain tuning, Adv. Electron. Mater. 1 (10) (2015), 1500190, https://doi.org/10.1002/aelm.201500190.
[50] R. Chaim, R. Marder, C. Estournés, Z. Shen, Densification and preservation of ceramic nanocrystalline character by spark plasma sintering, Adv. Appl. Ceram. 111 (5–6) (2012) 280–285, https://doi.org/10.1179/1743676111Y.0000000074.
[51] P. Radingoana, S. Guillemet-Fritsch, P. Olubambi, G. Chevallier, C. Estournès, Influence of processing parameters on the densification and the microstructure of pure zinc oxide ceramics prepared by spark plasma sintering, Ceram. Int. (2019), https://doi.org/10.1016/j.ceramint.2019.02.048.
[52] P. Cavaliere, B. Sadeghi, A. Shabani, Spark plasma sintering: process fundamentals, Spark plasma sintering of materials, Springer (2019) 3–20, https://doi.org/10.1007/978-3-030-05327-7_1.
[53] K.G. Ewsuk, D.T. Ellerby, C.B. DiAntonio, Analysis of nanocrystalline and microcrystalline ZnO sintering using master sintering curves, J. Am. Ceram. Soc. 89 (6) (2006) 2003–2009, https://doi.org/10.1111/j.1551-2916.2006.00990.x.
[54] N. Ma, J.-F. Li, B. Zhang, Y. Lin, L. Ren, G. Chen, Microstructure and thermoelectric properties of Zn1− xAlxO ceramics fabricated by spark plasma sintering, J. Phys. Chem. Solids 71 (9) (2010) 1344–1349, https://doi.org/10.1016/j.jpcs.2010.06.006.
[55] R. Chaim, G. Chevallier, A. Weibel, C. Estournès, Grain growth during spark plasma and flash sintering of ceramic nanoparticles: a review, J. Mater. Sci. 53 (5) (2018) 3087–3105, https://doi.org/10.1007/s10853-017 1761-7.
[56] P. Díaz-Chao, F. Giovannelli, O. Lebedev, D. Chateigner, L. Lutterotti, F. Delorme, E. Guilmeau, Textured Al-doped ZnO ceramics with isotropic grains, J. Eur. Ceram. Soc. 34 (16) (2014) 4247–4256, https://doi.org/10.1016/j.jeurceramsoc.2014.07.009.
[57] D. Bérardan, C. Byl, N. Dragoe, Influence of the preparation conditions on the thermoelectric properties of Al-doped ZnO, J. Am. Ceram. Soc. 93 (8) (2010) 2352–2358, https://doi.org/10.1111/j.1551-2916.2010.03751.x.
[58] S.I. Nunes, R.C. Bradt, Grain Growth of ZnO in ZnO-Bl2O3 Ceramics with Ai2O3, Addit., J. Am. Ceram. Soc. 78 (9) (1995) 2469–2475, https://doi.org/10.1111/j.1151-2916.1995.tb08687.x.
[59] H. Tomaszewski, Residual stresses in layered ceramic composites, J. Eur. Ceram. Soc. 19 (6–7) (1999) 1329–1331, https://doi.org/10.1016/S0955-2219(98)00428-2.
[60] Y. Pei, X. Shi, A. LaLonde, H. Wang, L. Chen, G.J. Snyder, Convergence of electronic bands for high performance bulk thermoelectrics, Nature 473 (7345) (2011) 66, https://doi.org/10.1038/nature09996.
[61] M. Søndergaard, E.D. Bøjesen, K.A. Borup, S. Christensen, M. Christensen, B. B. Iversen, Sintering and annealing effects on ZnO microstructure and thermoelectric properties, Acta Mater. 61 (9) (2013) 3314–3323, https://doi.org/10.1016/j.actamat.2013.02.021.
[62] S. Walia, S. Balendhran, H. Nili, S. Zhuiykov, G. Rosengarten, Q.H. Wang, M. Bhaskaran, S. Sriram, M.S. Strano, K. Kalantar-zadeh, Transition metal oxides–thermoelectric properties, Prog. Mater. Sci. 58 (8) (2013) 1443–1489, https://doi.org/10.1016/j.pmatsci.2013.06.003.